

The Synthesis of N-(Pyridin-2-yl)-Benzamides from Aminopyridine and Trans-Beta-Nitrostyrene by Fe₂Ni-BDC Bimetallic Metal-Organic Frameworks

Authors:

Trinh Duy Nguyen, Oanh Kim Thi Nguyen, Thuan Van Tran, Vinh Huu Nguyen, Long Giang Bach, Nhan Viet Tran, Dai-Viet N. Vo, Tuyen Van Nguyen, Seong-Soo Hong, Sy Trung Do

Date Submitted: 2019-12-16

Keywords: decarboxylative amidation, bimetallic metal-organic frameworks, metal-organic framework

Abstract:

A bimetallic metal-organic framework material, which was generated by bridging iron (III) cations and nickel (II) cations with 1,4-Benzenedicarboxylic anions (Fe₂Ni-BDC), was synthesized by a solvothermal approach using nickel (II) nitrate hexahydrate and iron (III) chloride hexahydrate as the mixed metal source and 1,4-Benzenedicarboxylic acid (H₂BDC) as the organic ligand source. The structure of samples was determined by X-ray powder diffraction (XRD), Fourier transform infrared spectroscopy (FT-IR), Raman spectroscopy, and nitrogen physisorption measurements. The catalytic activity and recyclability of the Fe₂Ni-BDC catalyst for the Michael addition amidation reaction of 2-aminopyridine and nitroolefins were estimated. The results illustrated that the Fe₂Ni-BDC catalyst demonstrated good efficiency in the reaction under optimal conditions. Based on these results, a reaction mechanism was proposed. When the molar ratio of 2-aminopyridine and trans-β-nitrostyrene was 1:1, and the solvent was dichloromethane, the isolated yield of pyridyl benzamide reached 82%; at 80 °C over 24 h. The catalyst can be reused without a substantial reduction in catalytic activity with 77% yield after six times of reuse.

Record Type: Published Article

Submitted To: LAPSE (Living Archive for Process Systems Engineering)

Citation (overall record, always the latest version):

LAPSE:2019.1598

Citation (this specific file, latest version):

LAPSE:2019.1598-1

Citation (this specific file, this version):






LAPSE:2019.1598-1v1

DOI of Published Version: <https://doi.org/10.3390/pr7110789>

License: Creative Commons Attribution 4.0 International (CC BY 4.0)

Article

The Synthesis of N-(Pyridin-2-yl)-Benzamides from Aminopyridine and Trans-Beta-Nitrostyrene by Fe₂Ni-BDC Bimetallic Metal–Organic Frameworks

Trinh Duy Nguyen ^{1,2,*} , Oanh Kim Thi Nguyen ^{1,2} , Thuan Van Tran ^{1,2} ,
Vinh Huu Nguyen ^{1,2} , Long Giang Bach ², Nhan Viet Tran ³, Dai-Viet N. Vo ¹ ,
Tuyen Van Nguyen ⁴, Seong-Soo Hong ⁵ and Sy Trung Do ⁴

¹ Center of Excellence for Green Energy and Environmental Nanomaterials (CE@GrEEN), Nguyen Tat Thanh University, 300A Nguyen Tat Thanh, Ho Chi Minh City 755414, Vietnam; kimoanhnguyen88@gmail.com (O.K.T.N.); tranuv@gmail.com (T.V.T.); nguyenuhuvinh3110@gmail.com (V.H.N.); vo.nguyen.dai.viet@gmail.com (D.-V.N.V.)

² NTT Institute of High Technology, Nguyen Tat Thanh University, 300A Nguyen Tat Thanh Street, Ho Chi Minh City 755414, Vietnam; blgiang@ntt.edu.vn

³ Faculty of Chemical Technology, Ho Chi Minh City University of Food Industry, 140 Le Trong Tan, Ho Chi Minh City 705800, Vietnam; nhantv25101997@gmail.com

⁴ Institute of Chemistry, Vietnam Academy of Science and Technology, 18 Hoang Quoc Viet, Hanoi 10072, Vietnam; ngvtuyen@hotmail.com (T.V.N.); dosyvh@gmail.com (S.T.D.)

⁵ Department of Chemical Engineering, Pukyong National University, 365 Shinsunro, Nam-ku, Busan 48547, Korea; sshong@pknu.ac.kr

* Correspondence: ndtrinh@ntt.edu.vn; Tel.: +84-971-275-356

Received: 28 June 2019; Accepted: 26 August 2019; Published: 1 November 2019



Abstract: A bimetallic metal–organic framework material, which was generated by bridging iron (III) cations and nickel (II) cations with 1,4-Benzenedicarboxylic anions (Fe₂Ni-BDC), was synthesized by a solvothermal approach using nickel (II) nitrate hexahydrate and iron (III) chloride hexahydrate as the mixed metal source and 1,4-Benzenedicarboxylic acid (H₂BDC) as the organic ligand source. The structure of samples was determined by X-ray powder diffraction (XRD), Fourier transform infrared spectroscopy (FT-IR), Raman spectroscopy, and nitrogen physisorption measurements. The catalytic activity and recyclability of the Fe₂Ni-BDC catalyst for the Michael addition amidation reaction of 2-aminopyridine and nitroolefins were estimated. The results illustrated that the Fe₂Ni-BDC catalyst demonstrated good efficiency in the reaction under optimal conditions. Based on these results, a reaction mechanism was proposed. When the molar ratio of 2-aminopyridine and trans-β-nitrostyrene was 1:1, and the solvent was dichloromethane, the isolated yield of pyridyl benzamide reached 82%; at 80 °C over 24 h. The catalyst can be reused without a substantial reduction in catalytic activity with 77% yield after six times of reuse.

Keywords: metal–organic framework; bimetallic metal–organic frameworks; decarboxylative amidation

1. Introduction

The amide bonds existing in a large number of structures and forming the backbone of the biologically essential proteins are the most basic building blocks of chemistry in nature [1]. The amide is also essential due to its role in the peptide bonds in pharmaceuticals, proteins, and natural products [1]. Amide bonds are characteristically synthesized by combining carboxylic acids and amines; however, the association of these two functional groups does not occur at room temperature [2]. Over the past decades, many researchers have proposed alternative synthesis methods, such as the Staudinger

reaction [3], direct amidation of aldehydes [4], transition-metal-catalyzed aminocarbonylation [5], and hydrating coupling of alkynes with azides [6], esters [7], alcohols [8], and alkynes with amines [9]. Pyridyl benzamides are one of the most critical types of N-heterocyclic amides and play an essential role in the composition of many important medicines (e.g., antiulcer agents, kinetoplastid inhibitors, antifungal agents, and luciferase inhibitors) [10]. Lately, the number of methods for the synthesis of pyridyl benzamides has been rising significantly. Typical examples include the Cu-catalyzed oxidation of methyl ketones [11], Cu-catalyzed oxidative coupling of 2-aminopyridines and terminal alkynes with visible light mediation [12], and the direct oxidative amidation reaction of aldehydes with amines [13]. Since N-heterocyclic amides are increasingly being used in medicine, the discovery of a more effective approach to synthesize pyridyl benzamides is of great importance in the medical industry and has thus been attempted via numerous routes. Xiao-Lan Xu et al. synthesized N-pyridinyl benzamide from benzoylformic acid and aniline using a transition metal catalyst, AgOTf [14]. Additionally, Leiling Deng et al. also created N-pyridinyl benzamide from 2-aminopyridine and phenylacetic acid in the presence of a Cu salt catalyst [15]. Very recently, Zhengwang Chen et al. performed a reaction to synthesize N-pyridinyl benzamide from 2-aminopyridine and *trans*- β -nitrostyrene by utilizing $\text{Ce}(\text{NO}_3)_3 \cdot 6\text{H}_2\text{O}$ catalyst in the absence of any oxidant or additive [16].

Metal–organic frameworks (MOFs), a class of porous materials with excellent potential, have been increasingly used in gas storage and separation because of their high capacity and selectivity properties [17]. MOF crystals are built through the formation of secondary building units (SBUs) consisting of organic linkers and metal ions/clusters. Numerous MOF structures have been designed to obtain different features such as enlarged surface areas [18], enhanced catalytic activity and electrical conductivity [19], better interaction at the open metal sites [20], and improved adsorption [21]. Notably, the application of MOFs as effective catalysts for organic reactions has received much attention [22]. MOFs with metal nodes (metal ions/clusters) can act as the active catalytic sites for many organic reactions such as oxidation reactions, C–C coupling reactions, and hydrogenation reactions. However, the fabrication of a MOF structure with high activity and selectivity still requires further investigation.

Recently, a new bimetallic metal–organic framework (BMOF) with a synergistic effect between different metal ions was developed. Different from the synthesis of MOFs where only one metal ion is combined with organic ligands, the synthesis process of a BMOF produces the pure phase of the BMOF by combining two different metal ions with organic ligands [23]. The BMOFs are expected to have improved stability, activity, and surface area and could be applicable in catalysis. For example, an Fe/Co mixed Hofmann MOF with coupling effects between Co^{2+} and Fe^{2+} ions was found to exhibit enhanced catalytic activity for an oxygen evolution reaction compared to that exhibited by the original single-metal MOFs [24]. Despite this, the catalysis applications of BMOFs have not been investigated so far.

The main aim of this study was to appraise the effect of a new BMOF (Fe_2Ni -1,4-Benzenedicarboxylic, Fe_2Ni -BDC) as a heterogeneous catalyst for organic synthesis reactions. Fe_2Ni -BDC was generated by bridging iron (III) cations and nickel (II) cations with 1,4-Benzenedicarboxylic anions (BDC^-) to create a porous three-dimensional structure [25,26]. We also investigated the synthesis of N-pyridinyl benzamide via the amidation process of *trans*- β -nitrostyrene and 2-aminopyridine using Fe_2Ni -BDC as an effective heterogeneous catalyst, without using added reducing agents or oxidizing agents. This catalyst might be reused for the creation of N-pyridinyl benzamide by the amidation reaction without significant depreciation in its efficiency. Fe_2Ni -BDC is also satisfactory from the view of green chemistry, as the solid catalyst used for the reaction can be easily recovered and reused. To the best of our knowledge, C=C double bond cleavage has not previously been performed using heterogeneous catalysis.

2. Experimental

2.1. Synthesis of the Catalyst

The bimetallic Fe/Ni-BDC catalyst was synthesized by the solvothermal method [27–29]. Typically, a clear solution containing H₂BDC (9 mmol, Sigma-Aldrich, Saint Louis, MO, USA), FeCl₃·6H₂O (6 mmol, Fisher Scientific, Hampton, NH, USA), and Ni(NO₃)₂·6H₂O (1.8 mmol, Fisher Scientific, Hampton, NH, USA) in 60 mL of *N,N*-dimethylformamide (DMF, 99%, Xilong Chemical Co., Ltd., Guangzhou, China) was prepared and placed in a pressure device (100 mL Hydrothermal Synthesis Autoclave Reactor 304 Stainless Steel High-Pressure Digestion Tank with PTFE Lining for Rapid Digestion of Insoluble Material, Baoshishan, Shanghai, China). Then, this device was placed in an oven (Mettler UN110, Schwabach, Germany) at 100 °C for three days. The non-reacted components, such as the remains of the organic linker in porous holes was eliminated by a distillation router with DMF solvent at 100 °C for a day. The orange solid was washed in DMF solvent (three times) and water (three times), followed by drying for a day at 60 °C. For comparison, Ni-BDC and Fe-BDC catalysts were also synthesized via the same method as for the synthesis of Fe₂Ni-BDC by using Ni(NO₃)₂·6H₂O for the synthesis of Ni-BDC and FeCl₃·6H₂O for the synthesis of Fe-BDC. The catalyst products obtained were an orange solid and a green solid for the Fe-BDC and Ni-BDC materials, respectively.

2.2. Catalyst Characterization

Physical and chemical methods are used to determine the characteristic properties of MOFs. X-ray diffraction (XRD) analysis was employed on a Bruker AXS D8 Advantage (Bruker, Billerica, MA, USA) operating with a Cu K α source to determine the material structure. The specific surface area and pore distribution of the obtained catalysts were determined using a Nova Quantachrome 2200e (Quantachrome Instruments, Kingville, TX, USA). Samples were activated in a vacuum at 150 °C for 6 h, followed by nitrogen adsorption at 77 °C and low pressure. Thermogravimetric analysis (TGA) was conducted on a Netzsch Thermoanalyzer STA 409 (Netzsch, Selb, Germany) with a heating rate of 10 °C/min from room temperature to 800 °C under inert gas conditions. The infrared spectrum (FT-IR) was attained using a Bruker TENSOR37 (Bruker, Billerica, MA, USA), and a KBr compressed sample was used to determine functional groups in the material. SEM images of the catalyst were obtained using a scanning electron microscope (SEM) on a JSM 7401F device (Jeol, Peabody, MA, USA).

2.3. The Synthesis of *N*-Pyridinyl Benzamide

In a typical catalytic experiment, *trans*- β -nitrostyrene (**1a**, 0.2 mmol, 0.0298 g) and 2-aminopyridine (**2a**, 0.2 mmol, 0.0188 g) in dichloromethane (DCM) solvent (1 mL) in the presence of Fe₂Ni-BDC were added into the pressure equipment. The reaction mixture was stirred at 80 °C for 24 h in atmospheric air (Table S1). Following this stage, the compound was cooled down to room temperature. The anticipated products were isolated using column chromatography. GC-MS, ¹H NMR, and ¹³C NMR analyses were employed to determine the product structure (Supplementary Materials). To assess the recovery and reusability of the catalyst, the catalyst was separated and washed thoroughly with large amounts of ethanol, dried at 100 °C, and reused for further experiments.

3. Results and Discussion

3.1. Characterization of the Ni-BDC, Fe-BDC, and Fe₂Ni-BDC Catalysts

In this study, a BMOF based on the coupling effects between Ni²⁺ and Fe²⁺ ions (Fe₂Ni-BDC) and the respective single-metal-ion MOFs (Ni-BDC and Fe-BDC) were obtained by direct synthesis with a clear solution containing nickel (II) nitrate hexahydrate and/or iron (III) chloride hexahydrate and terephthalic acid (H₂BDC) in dimethylformamide (DMF) solvent. Evidence of the formation of a MOF with bimetallic nodes was confirmed by X-ray powder diffraction (XRD), Fourier transform infrared spectroscopy (FT-IR), Raman spectroscopy, and nitrogen physisorption measurements.

The XRD patterns of the resulting Ni-BDC, Fe-BDC, and Fe₂Ni-BDC samples are shown in Figure S3 (Supplementary Materials). The pure Ni-BDC powder exhibited a similar XRD pattern (Figure S3a) to the previously reported ones synthesized by a solvothermal method with main diffraction peaks at 2θ of 11° , 11.5° , 14° , 15° , 16.5° , 17.5° , 28° , and 29° [27,28,30–32]. As can be observed in Figure 1b, the XRD patterns of the Fe-BDC exhibited peaks at 2θ of approximately of 9.2° , 9.5° , 14.0° , 16.4° , and 18.7° , and this result was also similar to the simulated patterns of MIL-53(Fe) previously reported in the literature [27,33]. Furthermore, the simulated diffraction patterns for the Ni- and Fe-based system (see Figures S1 and S2, Supplementary Materials) were exhibited. In the pattern of the Fe₂Ni-BDC samples (Figure S3c, Supplementary Materials), the XRD peaks emerged around 2θ of 7.4° , 8.8° , 9.2° , 9.8° , 16.7° , 18.7° , 17.8° , 20.0° , and 21.8° . It is clear that this result is also in line with those of the sample previously reported in the literature [25,26]. Besides this, no other diffraction peak combined with iron oxides, nickel oxides, or other diffraction peaks was found, proving the high purity of the samples. The XRD analytic results illustrate that the crystal structure of Fe₂Ni-BDC was substantially affected by the existence of assorted metal ions (Ni²⁺ and Fe³⁺ ions), and Fe₂Ni-BDC crystals could be formed by the combination of H₂BDC with Ni²⁺ and Fe³⁺ ions [25,26].

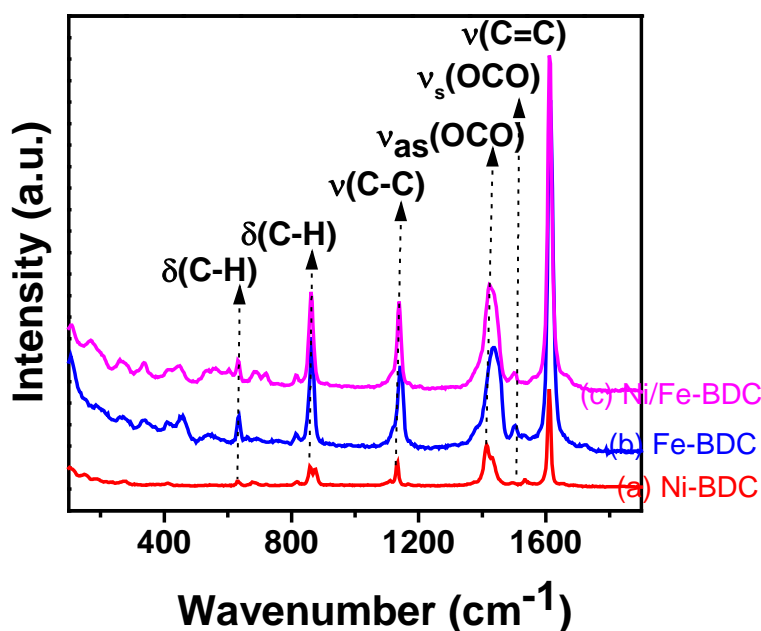


Figure 1. Raman spectroscopy of the Ni-1,4-Benzenedicarboxylic (Ni-BDC) (a), Fe-1,4-Benzenedicarboxylic (Fe-BDC) (b), and Fe₂Ni-1,4-Benzenedicarboxylic (Fe₂Ni-BDC) (c).

The FT-IR spectra of Ni-BDC, Fe-BDC, and Fe₂Ni-BDC are shown in Figure S4 (Supplementary Materials). The FT-IR spectra exhibited stretching vibration of the C=O bond at approximately 1680 cm^{-1} , while $\nu_{\text{asym}}(\text{OCO})$ and $\nu_{\text{sym}}(\text{OCO})$ bonds displayed stretching vibration at around 1601 cm^{-1} and 1391 cm^{-1} , respectively. Besides this, the FT-IR spectra displayed stretching vibration of the $\nu(\text{C-O})$ and $\delta(\text{C-H})$ bonds at 1017 cm^{-1} and 749 cm^{-1} (Figure S4A, Supplementary Materials). These results showed that the existence of the metal–ligand bond in the MOF structures. Particularly, the FT-IR spectrum of H₂BDC displayed no band at 1700 cm^{-1} . This result proves the absence of free H₂BDC in the MOF structures [34,35]. The feature bands of H₂O and DMF in the MOF materials were exhibited at 1657 cm^{-1} and 3387 cm^{-1} [25,26]. At lower frequencies, stretching vibration of the C–H bond, C=C bond, and –OCO function was observed at approximately 750 cm^{-1} , 690 cm^{-1} , and 660 cm^{-1} , respectively, proving the existence of the vibrations of the organic linker BDC (Figure S4B, Supplementary Materials) [26]. Moreover, it is clear that the strong band at 547 cm^{-1} may be attributed to either NiO vibrations or FeO vibrations [36]. The weak range at about 720 cm^{-1} is associated with

Fe_2NiO vibration, which was also detected in the $\text{Fe}_2\text{Ni-BDC}$ sample [26]. This result reinforces the notion that Ni^{2+} and Fe^{3+} ions may combine with H_2BDC to form $\text{Fe}_2\text{Ni-BDC}$ crystals.

The Raman spectroscopy results of Ni-BDC, Fe-BDC, and $\text{Fe}_2\text{Ni-BDC}$ are shown in Figure 1. Following previous studies, the symmetric oscillation modes and asymmetric oscillation of the COO-bond in the carboxylate group detected at approximately 1445 cm^{-1} and 1501 cm^{-1} may be the organic linker BDC in the metal-organic frameworks. The oscillation at around 1140 cm^{-1} can be attributed to the C-C bond of the carboxylate group with a benzene ring. Besides this, vibration of the C-H bond was observed at around 865 cm^{-1} and 630 cm^{-1} [25]. As shown in Figure 1, the presence of BDC ligand was also discovered in the catalyst sample, and no Raman sign corresponding to NiO, FeO, or other impurities was detected on the pattern, which is consistent with the X-ray diffraction results.

Concurrent thermal analysis permits simultaneous measurement of both the weight and heat flow alteration of Ni-BDC, Fe-BDC, and $\text{Fe}_2\text{Ni-BDC}$ powder in relation to the temperature under an air atmosphere. The patterns show the differential scanning calorimetry (DSC) and thermogravimetry (TGA) curves of Ni-BDC, Fe-BDC, and $\text{Fe}_2\text{Ni-BDC}$ powder from room temperature to $800\text{ }^\circ\text{C}$ under an air atmosphere (Figure 2). In the DSC curve of Ni-BDC, a powerful exothermic process occurred between $380\text{ }^\circ\text{C}$ and $480\text{ }^\circ\text{C}$, manifesting as a peak temperature at $450.57\text{ }^\circ\text{C}$ (Figure 2a). In the DSC curve of Fe-BDC, a robust exothermic process occurred between $260\text{ }^\circ\text{C}$ and $340\text{ }^\circ\text{C}$, illustrating a peak temperature at $316.53\text{ }^\circ\text{C}$ (Figure 2b). In the DSC curve of $\text{Fe}_2\text{Ni-BDC}$, a strongly exothermic process took place from $320\text{ }^\circ\text{C}$ to $490\text{ }^\circ\text{C}$, signified by a peak temperature at $437.99\text{ }^\circ\text{C}$ (Figure 2c). The weight loss occurring at temperatures below $200\text{ }^\circ\text{C}$ could be attributable to the vaporization of solvent (H_2O or DMF) obstructed within the frame, while the weight loss occurring between $200\text{ }^\circ\text{C}$ and $260\text{ }^\circ\text{C}$ is the result of the strong combining of H_2O or the frame of H_2O . A sudden weight loss may be discerned between 280 and $480\text{ }^\circ\text{C}$, conforming to a strongly exothermic process in the DSC curve. Herein, elemental analysis, i.e., EDX mapping and ICP analysis, can aid the identification of the Ni/Fe ratio in the bimetallic Ni/Fe-BDC MOF. Based on the results obtained from EDX mapping, we found that the proximate percentages of Ni and Fe were 5.7% and 11.2%, respectively (Figure S5, Supplementary Materials) or 1:2 when calculated in a molar ratio. Similarly, ICP analysis also indicated that the molar (atomic) ratio between Ni and Fe was at approximately 1:2. Therefore, it matched well with the formula of $\text{NiFe}_2\text{-BDC}$.

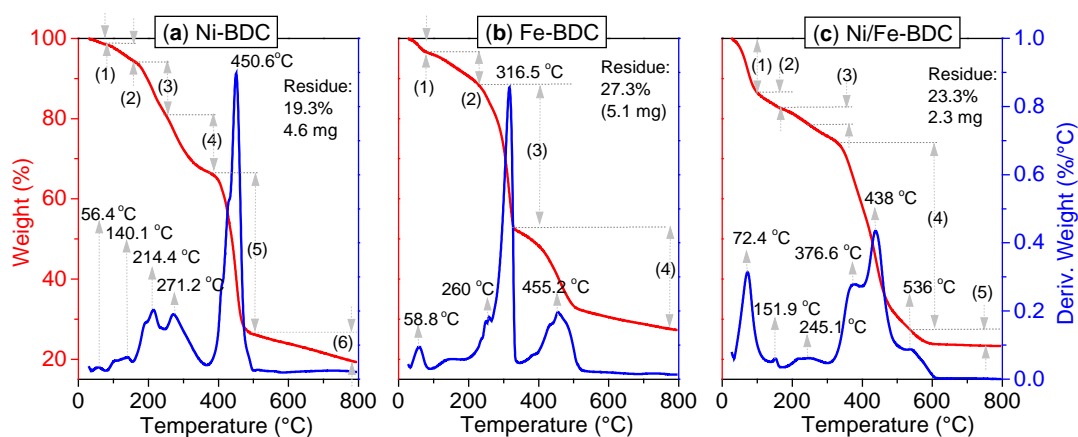


Figure 2. TGA analysis of the Ni-1,4-Benzenedicarboxylic (Ni-BDC) (a), Fe-1,4-Benzenedicarboxylic (Fe-BDC) (b), and $\text{Fe}_2\text{Ni-1,4-Benzenedicarboxylic}$ ($\text{Fe}_2\text{Ni-BDC}$) (c).

The morphology, size, and regularity of the Ni-BDC, Fe-BDC, and $\text{Fe}_2\text{Ni-BDC}$ samples were studied by SEM (Figure 3). The Ni-BDC sample includes stacked planar sheets with a size up to several micrometers (Figure 3a). The shape of pure Fe-BDC showed two types of particles: bigger, rod-like particles and other, smaller, pseudo-spherical particles (Figure 3b). The SEM pictures of the particles unveiled the creation of uniform micro-sized hexagonal rods (Figure 3c). Besides this, the $\text{Fe}_2\text{Ni-BDC}$ sample consists of stacked planar sheets and other smaller pseudo-spherical particles.

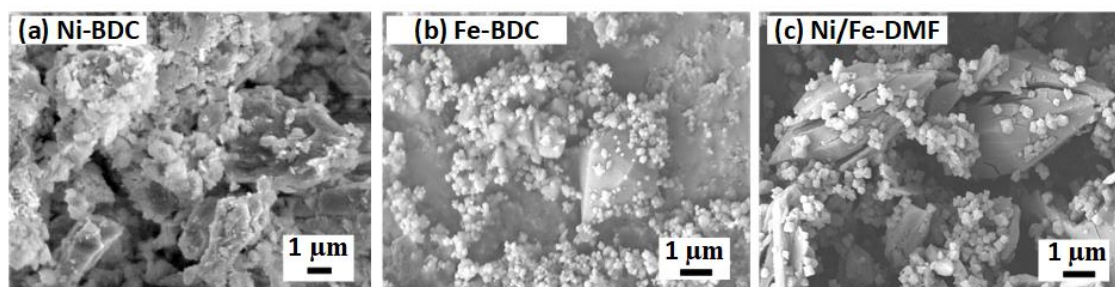


Figure 3. SEM images of Ni-1,4-Benzenedicarboxylic (Ni-BDC) (a), Fe-1,4-Benzenedicarboxylic (Fe-BDC) (b), and Fe₂Ni-1,4-Benzenedicarboxylic (Fe₂Ni-BDC) (c).

The surface areas of the catalysts were confirmed by nitrogen adsorption–desorption isotherms derived from Brunauer–Emmett–Teller (BET). The isotherms of Ni-BDC, Fe-BDC, and Fe₂Ni-BDC are presented in Figure 4. The BET surface areas of Fe-BDC and Fe₂Ni-BDC were 158 m²/g and 247 m²/g, respectively. Meanwhile, the BET surface area of Ni-BDC was extremely low at around 2.28 m²/g, and it does not seem to be porous. The mesopore size distribution curves of specimens calculated using the Barrett–Joyner–Halenda (BJH) model are displayed in Figure 4. The pore volume and pore width of Ni-BDC, Fe-BDC, and Fe₂Ni-BDC suggested average pore sizes of about 25 nm, 11 nm, and 13 nm, respectively. Based on the above results, including XRD, FT-IR, Raman, DSC, TGA, and BET, we conclude that an Fe₂Ni-BDC bimetallic metal–organic framework was successfully synthesized by the solvothermal approach.

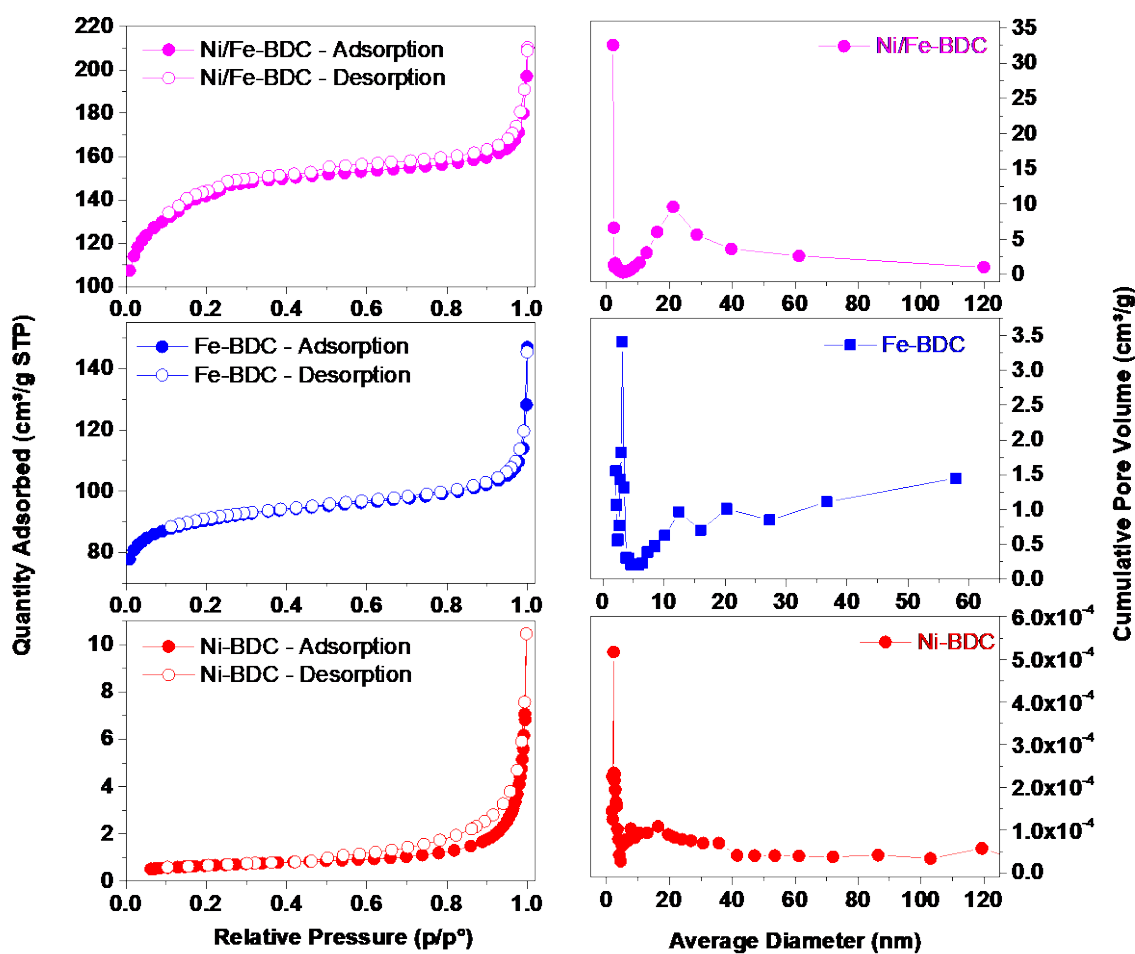
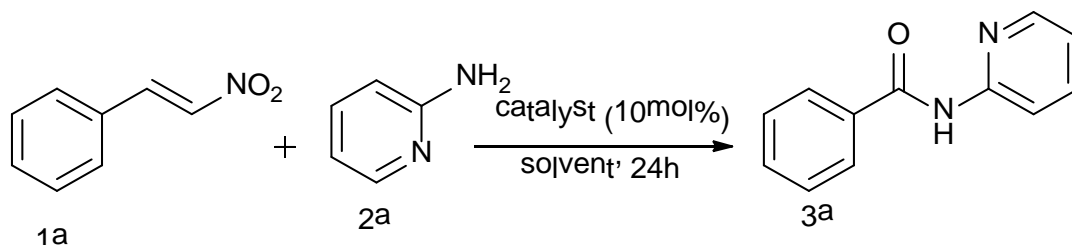


Figure 4. N₂ adsorption–desorption isotherms (left) and pore size distributions (right) of metal–organic framework (MOF) samples.

3.2. The Synthesis of *N*-Pyridinyl Benzamide

Scheme 1 illustrates the amidation reaction between *trans*- β -nitrostyrene and 2-aminopyridine using catalysts $\text{Ni}(\text{NO}_3)_2 \cdot 6\text{H}_2\text{O}$, $\text{FeCl}_3 \cdot 6\text{H}_2\text{O}$, Ni-BDC, Fe-BDC, and Fe_2Ni -BDC. The performance of the reactions with different metal-centered catalysts demonstrated that Fe_2Ni -BDC resulted in the best activity for this amidation process (Figure 5a, Table S1).



Scheme 1. The amidation reaction between *trans*- β -nitrostyrene and 2-aminopyridine using Fe_2Ni -BDC as a catalyst.

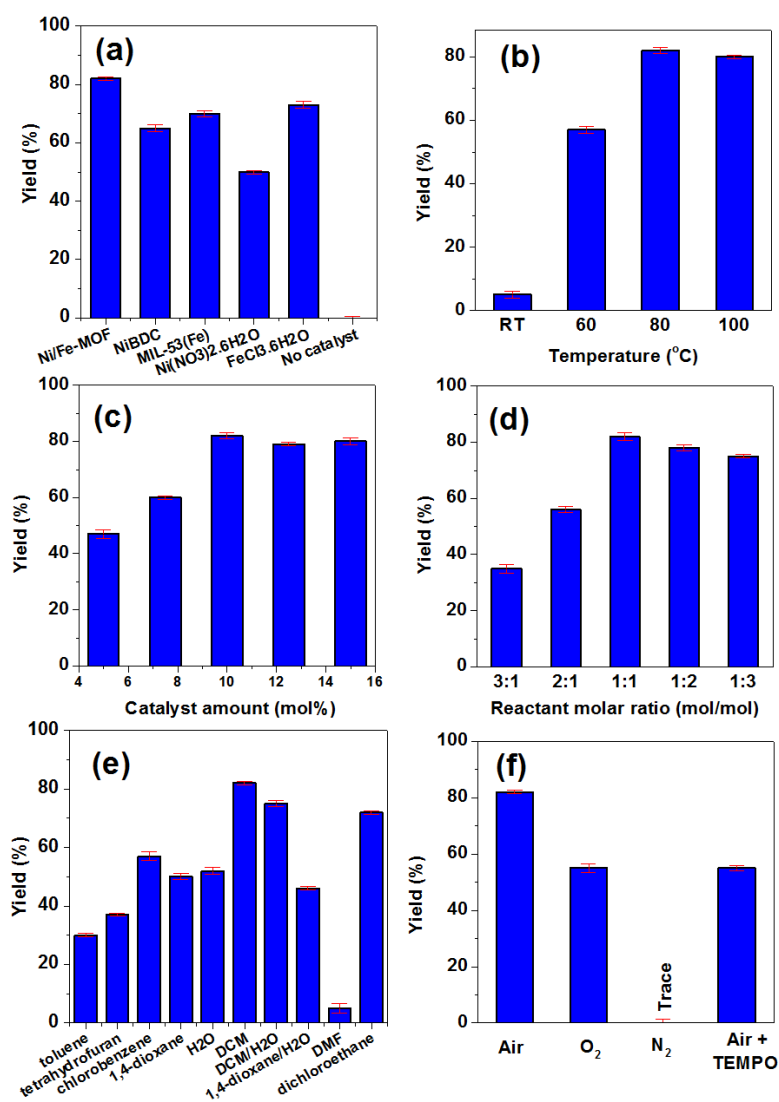


Figure 5. The yield of *N*-pyridinyl benzamide vs. catalyst (a), temperature (b), catalyst amount (c), reaction molar ratio (d), solvents (e), and yield of *N*-pyridinyl benzamide under air, O_2 , N_2 , and air + 2,2,6,6-Tetramethyl-1-piperidinyloxy (TEMPO) (f).

The amidation reaction was performed at different temperatures from room temperature to 100 °C. The results (Figure 5b and Table S1) indicated that lower temperature led to a decline in product yield, and the reaction occurred when the mixture was heated. Also, when this reaction was carried out at 100 °C, a lower yield of product **3a** was observed, which could result from the decomposition of reactants and products, adversely affecting the reaction process. The yield of product **3a** reached its highest value when the reaction was carried out at 80 °C; therefore, 80 °C was chosen as the optimal reaction temperature for further studies.

Figure 5c shows the effect of catalyst amount (mol %) on the yield of product **3a**. These results revealed that the yield of **3a** reached a peak (82%) when using 10 mol % catalyst. This behavior necessitates the bimetallic framework for catalyzing the alteration. The use of BMOF catalyst for the reaction brought about a remarkable progression in the reaction yield. The reaction utilizing 5 mol % of catalyst might achieve around 47% yield, and this yield figure could be improved to 60% yield if 7.5 mol % catalyst is used. However, the use of more than 10 mol % catalyst seemed to be redundant because the yield of **3a** was not improved substantially above this concentration (Table S1).

We also investigated the effect of the *trans*- β -nitrostyrene/2-aminopyridine molar ratio on the production of *N*-(pyridin-2-yl)-benzamide. The reaction was carried at 80 °C under air in DCM for 24 h in the presence of 10 mol % of catalyst. The survey data illustrated that the reactant molar ratio exerted a significant effect on the yield of product **3a**. The reaction utilizing the proportion of 1 equivalent of **1a** achieved 82% yield in air. The excess **1a** reactant resulted in a reduced yield of **3a**. Indeed, as the yield of the product reached 56%, the molar proportion of reactants in the reaction approximated 2:1. However, the yield was decreased drastically to merely 35% when 3 equivalents of **1a** were used. It was clear that excess **2a** was preferred in the reaction. The yield of product **3a** reached approximately 78% after 24 h with a reactant molar proportion of either 1:2 or 1:3. However, the optimal yield of **3a** was attained at the reactant molar proportion of 1:1 (Figure 5d, Table S1).

Because the amidation reaction of **1a** and **2a** was carried out in the liquid phase, we needed to examine the effect of solvents on the catalytic activity. In the first report of the synthesis of *N*-(pyridin-2-yl)-benzamide derivatives from **1a** and **2a**, Zhengwang Chen et al. [16] implemented the reaction in various co-solvents and illustrated that co-solvent H₂O/dioxane could improve the yield of products. The effect of solvents such as toluene, DMF, 1,4-dioxane, tetrahydrofuran (THF), chlorobenzene, DCM/H₂O, dioxane/H₂O, H₂O, and dichloroethane on the yield of **3a** was investigated. As shown in Figure 5e and Table S1, DMF solvent was unsuitable for the reaction utilizing the bimetallic framework catalyst, with only 5% yield of **3a** after 24 h. The yields of product **3a** were higher in toluene and tetrahydrofuran—30% and 37% yields, respectively, after 24 h. The reactions controlled in dioxane, dioxane/H₂O, H₂O, and chlorobenzene produced **3a** in yields of 52%, 46%, 50%, and 57%, respectively. Higher yields of 75% and 72% were obtained for DCM/H₂O and dichloroethane. Among the aforementioned solvents, DCM gave the best result with an 82% yield of **3a** after 24h (Figure 5e and Table S1).

As shown in Figure 5f, the production of **3a** was not detected when the reaction was conducted under N₂ gas, highlighting the essential role of O₂ in the reaction. Further investigation of the reaction with the bimetallic framework catalyst under O₂ illustrating the role of the Fe₂Ni-BDC catalyst was not feasible. Besides this, the reaction that was carried out in the presence of 2,2,6,6-Tetramethyl-1-piperidinyloxy (TEMPO) revealed no obvious prevention of the reaction, allowing us to propose a probably easier radical path in this amidation reaction (Figure 5f, Table S1). After some surveys, we determined that the appropriate reaction conditions are as follows: *trans*- β -nitrostyrene (**1a**, 0.2 mmol), 2-aminopyridine (**2a**, 0.2 mmol), catalyst (10 mol %), and DCM (1 mL) at 80 °C for 24 h.

A leaching evaluation was employed to confirm whether the active sites going into solution from the solid catalyst could accelerate the creation of *N*-(pyridin-2-yl)-benzamide, as the leaching phenomenon could happen throughout the stages of the reaction. The reaction was performed at 80 °C in DCM solvent for 24 h, with reactants consisting of *trans*-1-nitro-phenylethylene and 2-pyridyl amine and with 10 mol % catalyst under air atmosphere. After the initial 4 h stage with 12% yield recorded,

the catalyst was separated by centrifugation. Then, new reactants were added to the solution phase in a clean, pressurized vial with magnetic stirring and the temperature maintained at 80 °C for 24 h. It was observed that the formation of N-(pyridin-2-yl)-benzamide stopped after the catalyst was separated (Figure 6a). These figures indicate that the amidation of *trans*-1-nitro-phenylethylene with 2-aminopyridine to generate N-(pyridin-2-yl)-benzamide could be maintained only in the presence of the solid catalyst.

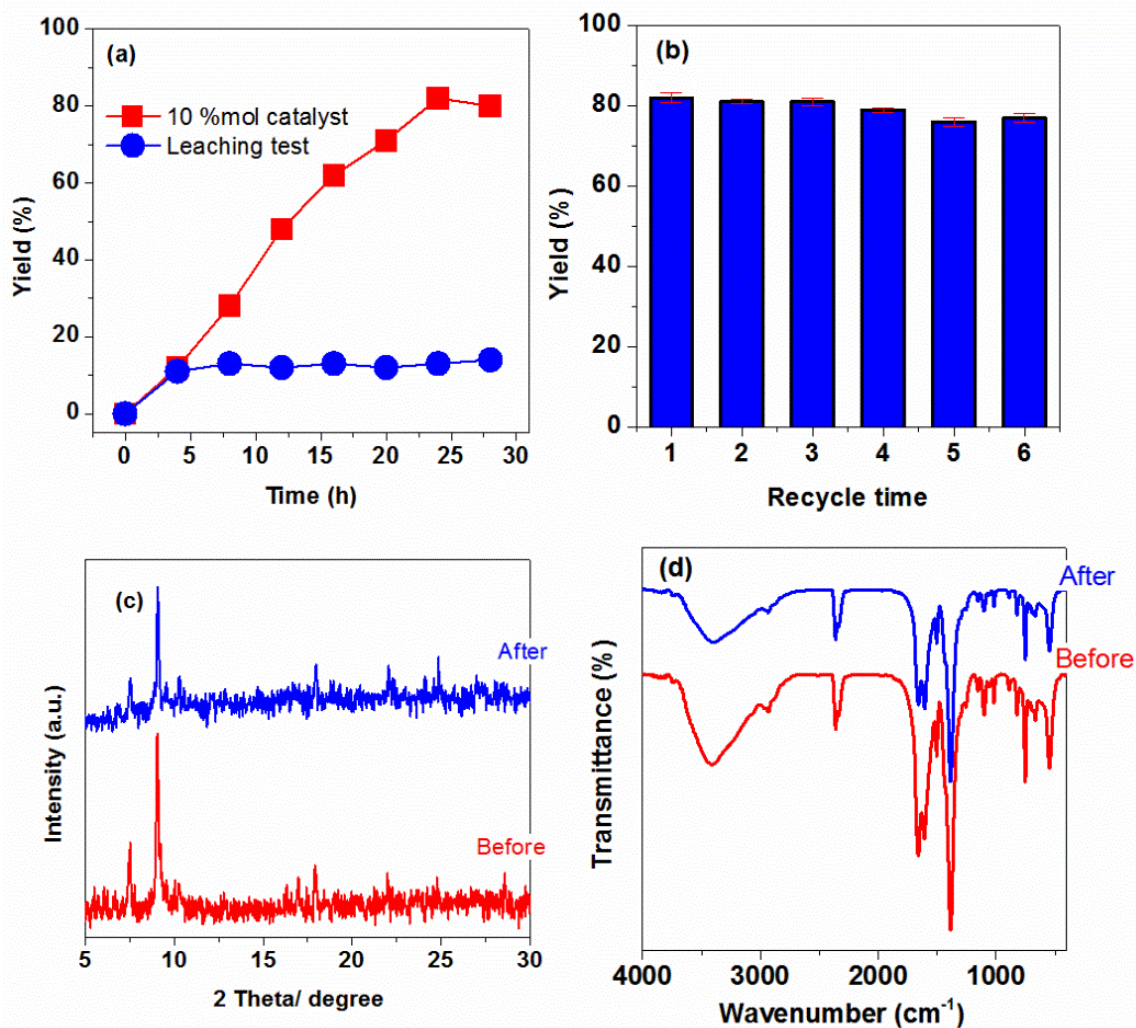
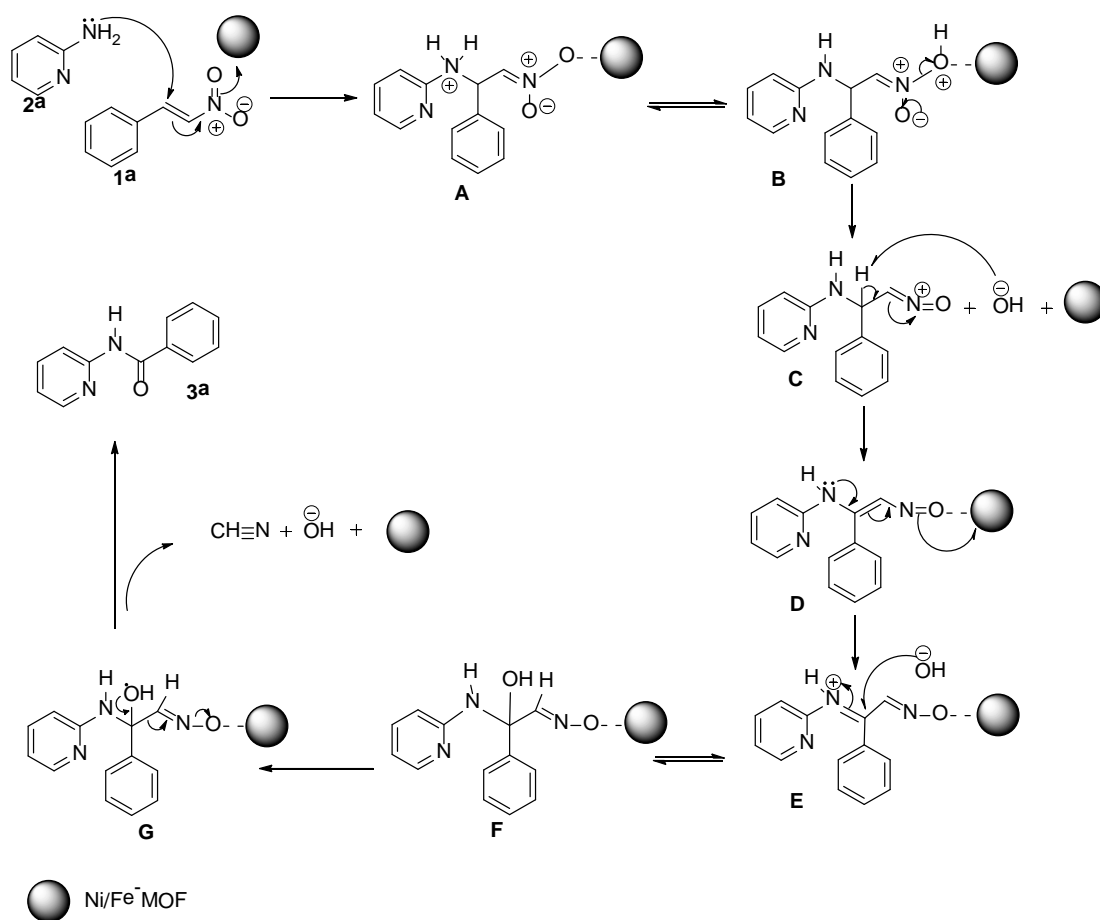


Figure 6. Leaching test (a), catalyst reusability (b), XRD pattern (c), and FT-IR spectroscopy (d) of the fresh and recovered catalyst.

Another striking feature that differentiates heterogeneous catalysis from homogeneous catalysis is the capability of the catalyst to be recovered and recycled. The catalyst was appropriately surveyed for recyclability in the reaction over six successive runs. The reaction was performed under optimal conditions at 80 °C in an air atmosphere. Upon completion of the first run, the catalyst was separated, washed cautiously with DCM and DMF, and dried at 100 °C for 3 h. Afterward, the recovered catalyst was recycled in new experiments. After the experiments were conducted, these data demonstrated that the catalyst might be recycled numerous times in the reaction of 2-aminopyridine and *trans*-1-nitro-phenylethylene to create N-(pyridin-2-yl)-benzamide without significantly compromising the yield. The yield of N-(pyridin-2-yl)-benzamide noted in the sixth run was 77% (Figure 6b). Moreover, the whole catalyst might be withheld after the reaction process, as shown by XRD (Figure 6c) and FT-IR (Figure 6d) spectroscopy of the recovered BMOFs.

Based on the experimental results, a reasonable mechanism is suggested in Scheme 2. Initially, the intermediary A was created via the Michael addition of *trans*- β -nitrostyrene **1a** and 2-pyridine amines **2a** as a nucleophile. When the catalyst played the role of a Lewis acid, the intermediary A was able to form a bond covalent with the O molecule on the nitro group, permitting the Michael addition, because the Fe^{3+} and Ni^{2+} ions in the BMOFs had many empty orbitals in the molecule. Intermediary C formed through successive dehydration of B and was reorganized to imine intermediary D. Following that, hydration of E brought about the intermediary F. After that, protonation of F took place by dehydration to provide the α -aminonitrile to intermediary G. Eventually, the target product **3a** was formed via a nucleophilic addition and elimination process. Via this proposed mechanism, the catalyst with two active metal centers improved the reaction yield. Therefore, the catalysis activity of $\text{Fe}_2\text{Ni-BDC}$ was enhanced when compared with the catalysis activity of the single-metal centers of Ni-BDC and Fe-BDC.

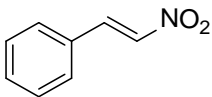
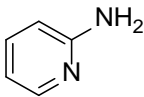
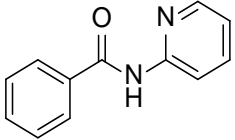
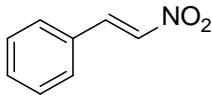
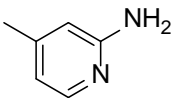
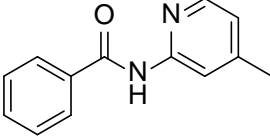
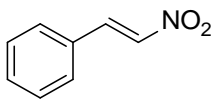
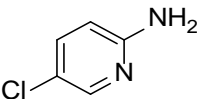
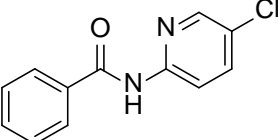
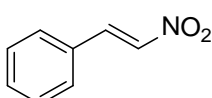
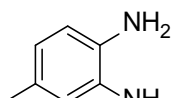
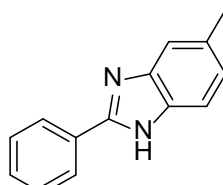
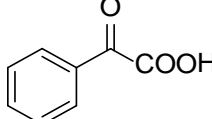
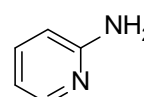
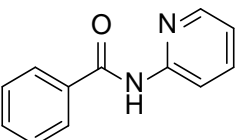


Scheme 2. Proposed reaction mechanism.

The study was subsequently extended to the synthesis of various N-(pyridin-2-yl)benzamide derivatives. The reactions were conducted between derivatives of 2-aminopyridine and *trans*- β -nitrostyrene in DCM solvent for 24 h under air atmosphere at 80 °C with 10 mol % of the catalyst. The products were purified by column chromatography, and isolated yields were noted. As shown in Table 1, N-(pyridin-2-yl)benzamide was created with 82% yield (entry 1, Table 1, Figures S6 and S7). The existence of a substituent on the pyridine ring in 2-aminopyridine reduced the yield slightly. The reaction performed between 4-methyl-2-aminopyridine and *trans*- β -nitrostyrene produced N-(4-methylpyridin-2-yl)benzamide with 78% yield (entry 2, Table 1, Figures S8 and S9), while a 68% yield of N-(5-chloropyridin-2-yl)benzamide was obtained for a reaction between 5-chloro-2-aminopyridine and *trans*- β -nitrostyrene (entry 3, Table 1, Figures S10 and S11). Besides these,

the reaction conducted between 4-methyl-o-phenylenediamine and *trans*- β -nitrostyrene produced 5-methyl-2-phenyl-1*H*-benzo[*d*]imidazole with 63% yield (entry 4, Table 1, Figures S12 and S13). Finally, N-(pyridin-2-yl)-benzamide was still generated when the reaction was performed between benzoylformic acid and 2-aminopyridine with 74% yield (entry 5, Table 1, Figures S14 and S15).

Table 1. Synthesis of different N-(pyridin-2-yl)-benzamide derivatives utilizing Fe₂Ni-BDC catalyst.

| Entry | Reactant 1 | Reactant 2 | Product | Isolated Yields (%) |
|-------|---|---|--|---------------------|
| 1 |  |  |  | 82 (85 [16]) |
| 2 |  |  |  | 78 |
| 3 |  |  |  | 68 |
| 4 |  |  |  | 63 |
| 5 |  |  |  | 74 |

4. Conclusions

The bimetallic metal–organic framework Fe₂Ni-BDC is a productive heterogeneous catalyst for the amidation reaction between *trans*-1-nitro-phenylethylene and 2-aminopyridine to create N-(pyridin-2-yl)-benzamide under air. Fe₂Ni-BDC showed higher productivity in the synthesis of N-(pyridin-2-yl)-benzamide than other metal–organic frameworks. The bimetallic metal–organic framework was surveyed as a heterogeneous catalyst for the amidation reaction. The catalyst was successfully recovered and reused for the reaction generating N-(pyridin-2-yl)-benzamide without a reduction in catalyst activity. To the best of our knowledge, the formation of N-(pyridin-2-yl)-benzamide has not been previously achieved utilizing a heterogeneous catalyst.

Supplementary Materials: The following are available online at <http://www.mdpi.com/2227-9717/7/11/789/s1>: 1. General experimental information. 2. General procedure for the synthesis of N-pyridyl benzamide. 3. General procedure of investigation for the synthesis of N-pyridinyl benzamide. 4. Characterization data for all products. Table S1: Optimization of reaction conditions. Figure S1: The presented simulated diffraction patterns for Ni-based was based on the corresponding check CIF file of Ni-BDC compare with experimental patterns. Figure S2: The presented simulated diffraction patterns for Fe-based was based on the corresponding check CIF file of MIL-53 (Fe) compare with experimental patterns. Figure S3: X-ray powder diffraction of Ni-BDC, Fe-BDC and Fe₂Ni-BDC. Figure S4: FT-IR spectra of the Ni-BDC, Fe-BDC, and Fe₂Ni-BDC. Figure S5: EDX mapping point of Fe₂Ni-BDC. Figure S6: ¹H-NMR spectra of N-(pyridin-2-yl)benzamide. Figure S7: ¹³C-NMR spectra of N-(pyridin-2-yl)benzamide.

Figure S8: ^1H -NMR spectra of N-(4-methylpyridin-2-yl)benzamide. Figure S9: ^{13}C -NMR spectra of N-(4-methylpyridin-2-yl)benzamide. Figure S10: ^1H -NMR spectra of 5-methyl-2-phenyl-1H-benzo[d]imidazole. Figure S11: ^{13}C -NMR spectra of 5-methyl-2-phenyl-1H-benzo[d]imidazole. Figure S12: ^1H -NMR spectra of N-(5-chloropyridin-2-yl)benzamide. Figure S13: ^{13}C -NMR spectra of N-(5-chloropyridin-2-yl)benzamide. Figure S14: ^1H -NMR spectra of N-(pyridin-2-yl)benzamide. Figure S15: ^{13}C -NMR spectra of N-(pyridin-2-yl)benzamide.

Author Contributions: Data curation, O.K.T.N., V.H.N. and N.V.T.; Formal analysis, T.V.T. and S.T.D.; Methodology, T.V.T., V.H.N., N.V.T. and T.V.N.; Supervision, T.D.N.; Writing—original draft, O.K.T.N.; Writing—review and editing, L.G.B., D.-V.N.V., T.V.N., S.-S.H. and S.T.D.

Funding: This work was supported by the Vietnam National Foundation for Science and Technology Development (NAFOSTED) under grant number 104.01-2019.16.

Conflicts of Interest: The authors declare no conflict of interest.

References

1. Lundberg, H.; Tinnis, F.; Selander, N.; Adolfsson, H. Catalytic amide formation from non-activated carboxylic acids and amines. *Chem. Soc. Rev.* **2014**, *43*, 2714–2742. [[CrossRef](#)] [[PubMed](#)]
2. Valeur, E.; Bradley, M. Amide bond formation: Beyond the myth of coupling reagents. *Chem. Soc. Rev.* **2009**, *38*, 606–631. [[CrossRef](#)] [[PubMed](#)]
3. Köhn, M.; Breinbauer, R. The Staudinger ligation—A gift to chemical biology. *Angew. Chem. Int. Ed.* **2004**, *43*, 3106–3116. [[CrossRef](#)] [[PubMed](#)]
4. Leow, D. Phenazinium salt-catalyzed aerobic oxidative amidation of aromatic aldehydes. *Org. Lett.* **2014**, *16*, 5812–5815. [[CrossRef](#)]
5. Fang, X.; Li, H.; Jackstell, R.; Beller, M. Selective palladium-catalyzed aminocarbonylation of 1,3-dienes: Atom-efficient synthesis of β,γ -unsaturated amides. *J. Am. Chem. Soc.* **2014**, *136*, 16039–16043. [[CrossRef](#)]
6. Cassidy, M.P.; Raushel, J.; Fokin, V.V. Practical synthesis of amides from in situ generated copper(I) acetylides and sulfonyl azides. *Angew. Chem. Int. Ed.* **2006**, *45*, 3154–3157. [[CrossRef](#)]
7. Morimoto, H.; Fujiwara, R.; Shimizu, Y.; Morisaki, K.; Ohshima, T. Lanthanum(III) triflate catalyzed direct amidation of esters. *Org. Lett.* **2014**, *16*, 2018–2021. [[CrossRef](#)]
8. Liu, X.; Jensen, K.F. Multistep synthesis of amides from alcohols and amines in continuous flow microreactor systems using oxygen and urea hydrogen peroxide as oxidants. *Green Chem.* **2013**, *15*, 1538–1541. [[CrossRef](#)]
9. Chen, Z.W.; Jiang, H.F.; Pan, X.Y.; He, Z.J. Practical synthesis of amides from alkynyl bromides, amines, and water. *Tetrahedron* **2011**, *67*, 5920–5927. [[CrossRef](#)]
10. Ferrins, L.; Gazdik, M.; Rahmani, R.; Varghese, S.; Sykes, M.L.; Jones, A.J.; Avery, V.M.; White, K.L.; Ryan, E.; Charman, S.A.; et al. Pyridyl benzamides as a novel class of potent inhibitors for the kinetoplastid *Trypanosoma brucei*. *J. Med. Chem.* **2014**, *57*, 6393–6402. [[CrossRef](#)]
11. Subramanian, P.; Indu, S.; Kaliappan, K.P. A one-pot copper catalyzed biomimetic route to *n*-heterocyclic amides from methyl ketones via oxidative C–C bond cleavage. *Org. Lett.* **2014**, *16*, 6212–6215. [[CrossRef](#)] [[PubMed](#)]
12. Ragupathi, A.; Sagadevan, A.; Lin, C.C.; Hwu, J.R.; Hwang, K.C. Copper(I)-catalyzed oxidative C–N coupling of 2-aminopyridine with terminal alkynes featuring a C–C bond cleavage promoted by visible light. *Chem. Commun.* **2016**, *52*, 11756–11759. [[CrossRef](#)] [[PubMed](#)]
13. Patel, O.P.S.; Anand, D.; Maurya, R.K.; Yadav, P.P. Copper-catalyzed highly efficient oxidative amidation of aldehydes with 2-aminopyridines in an aqueous micellar system. *Green Chem.* **2015**, *17*, 3728–3732. [[CrossRef](#)]
14. Xu, X.L.; Xu, W.T.; Wu, J.W.; He, J.B.; Xu, H.J. Silver-promoted decarboxylative amidation of α -keto acids with amines. *Org. Biomol. Chem.* **2016**, *14*, 9970–9973. [[CrossRef](#)] [[PubMed](#)]
15. Deng, L.; Huang, B.; Liu, Y. Copper(II)-mediated, carbon degradation-based amidation of phenylacetic acids toward *N*-substituted benzamides. *Org. Biomol. Chem.* **2018**, *16*, 1552–1556. [[CrossRef](#)] [[PubMed](#)]
16. Chen, Z.; Wen, X.; Qian, Y.; Liang, P.; Liu, B.; Ye, M. Ce(III)-catalyzed highly efficient synthesis of pyridyl benzamides from aminopyridines and nitroolefins without external oxidants. *Org. Biomol. Chem.* **2018**, *16*, 1247–1251. [[CrossRef](#)]
17. Yang, X.; Xu, Q. Bimetallic metal-organic frameworks for gas storage and separation. *Cryst. Growth Des.* **2017**, *17*, 1450–1455. [[CrossRef](#)]

18. Xia, B.Y.; Yan, Y.; Li, N.; Wu, H.B.; Lou, X.W.D.; Wang, X. A metal-organic framework-derived bifunctional oxygen electrocatalyst. *Nat. Energy* **2016**, *1*, 15006. [[CrossRef](#)]
19. Chen, W.; Zhang, Z.; Bao, W.; Lai, Y.; Li, J.; Gan, Y.; Wang, J. Hierarchical mesoporous γ -Fe₂O₃/carbon nanocomposites derived from metal organic frameworks as a cathode electrocatalyst for rechargeable Li-O₂ batteries. *Electrochim. Acta* **2014**, *134*, 293–301. [[CrossRef](#)]
20. Kim, S.H.; Lee, Y.J.; Kim, D.H.; Lee, Y.J. Bimetallic metal-organic frameworks as efficient cathode catalysts for Li-O₂ batteries. *ACS Appl. Mater. Interfaces* **2018**, *10*, 660–667. [[CrossRef](#)]
21. Villajos, J.A.; Orcajo, G.; Martos, C.; Botas, J.Á.; Villacañas, J.; Calleja, G. Co/Ni mixed-metal sited MOF-74 material as hydrogen adsorbent. *Int. J. Hydrog. Energy* **2015**, *40*, 5346–5352. [[CrossRef](#)]
22. Alberio, J.; García, H. Metal organic frameworks as catalysts for organic reactions. In *New Materials for Catalytic Applications*; Elsevier: Amsterdam, The Netherlands, 2016; pp. 13–40. ISBN 9780444635877.
23. Gholipour-Ranjbar, H.; Soleimani, M.; Naderi, H.R. Application of Ni/Co-based metal-organic frameworks (MOFs) as an advanced electrode material for supercapacitors. *New J. Chem.* **2016**, *40*, 9187–9193. [[CrossRef](#)]
24. Gao, J.; Cong, J.; Wu, Y.; Sun, L.; Yao, J.; Chen, B. Bimetallic hofmann-type metal-organic framework nanoparticles for efficient electrocatalysis of oxygen evolution reaction. *ACS Appl. Energy Mater.* **2018**, *1*, 5140–5144. [[CrossRef](#)]
25. Vuong, G.T.; Pham, M.H.; Do, T.O. Direct synthesis and mechanism of the formation of mixed metal Fe₂Ni-MIL-88B. *CrystEngComm* **2013**, *15*, 9694–9703. [[CrossRef](#)]
26. Vuong, G.T.; Pham, M.H.; Do, T.O. Synthesis and engineering porosity of a mixed metal Fe₂Ni MIL-88B metal-organic framework. *Dalton Trans.* **2013**, *42*, 550–557. [[CrossRef](#)]
27. Trinh, N.D.; Hong, S.-S. Photocatalytic decomposition of methylene blue over MIL-53(Fe) prepared using microwave-assisted process under visible light irradiation. *J. Nanosci. Nanotechnol.* **2014**, *15*, 5450–5454. [[CrossRef](#)]
28. Nguyen, V.; Nguyen, T.; Bach, L.; Hoang, T.; Bui, Q.; Tran, L.; Nguyen, C.; Vo, D.-V.; Do, S. Effective photocatalytic activity of mixed Ni/Fe-base metal-organic framework under a compact fluorescent daylight lamp. *Catalysts* **2018**, *8*, 487. [[CrossRef](#)]
29. Schejn, A.; Falk, V.; Mozet, K.; Schneider, R.; Aboulaich, A.; Balan, L.; Lalevée, J.; Medjahdi, G.; Aranda, L. Cu²⁺-doped zeolitic imidazolate frameworks (ZIF-8): Efficient and stable catalysts for cycloadditions and condensation reactions. *Catal. Sci. Technol.* **2015**, *5*, 1829–1839. [[CrossRef](#)]
30. Wu, M.S.; Chen, F.Y.; Lai, Y.H.; Sie, Y.J. Electrocatalytic oxidation of urea in alkaline solution using nickel/nickel oxide nanoparticles derived from nickel-organic framework. *Electrochim. Acta* **2017**, *258*, 167–174. [[CrossRef](#)]
31. Wu, M.S.; Chen, C.Y.; Chen, Y.R.; Shih, H.C. Synthesis of bimodal mesoporous carbon with embedded nickel nanoparticles through pyrolysis of nickel-organic framework as a counter-electrode catalyst for dye-sensitized solar cells. *Electrochim. Acta* **2016**, *215*, 50–56. [[CrossRef](#)]
32. Nguyen, V.H.; Bach, L.G.; Do, S.T.; Thuong, N.T.; Nguyen, T.D. Photoluminescence properties of Eu-doped MIL-53(Fe) obtained by solvothermal synthesis. *J. Nanosci. Nanotechnol.* **2018**, *19*, 1148–1150. [[CrossRef](#)] [[PubMed](#)]
33. Haque, E.; Khan, N.A.; Park, H.J.; Jhung, S.H. Synthesis of a metal-organic framework material, iron terephthalate, by ultrasound, microwave, and conventional electric heating: A kinetic study. *Chem. A Eur. J.* **2010**, *16*, 1046–1052. [[CrossRef](#)] [[PubMed](#)]
34. Sun, Q.; Liu, M.; Li, K.; Han, Y.; Zuo, Y.; Chai, F.; Song, C.; Zhang, G.; Guo, X. Synthesis of Fe/M (M = Mn, Co, Ni) bimetallic metal organic frameworks and their catalytic activity for phenol degradation under mild conditions. *Inorg. Chem. Front.* **2017**, *4*, 144–153. [[CrossRef](#)]
35. Vu, T.A.; Le, G.H.; Dao, C.D.; Dang, L.Q.; Nguyen, K.T.; Nguyen, Q.K.; Dang, P.T.; Tran, H.T.K.; Duong, Q.T.; Nguyen, T.V.; et al. Arsenic removal from aqueous solutions by adsorption using novel MIL-53(Fe) as a highly efficient adsorbent. *RSC Adv.* **2015**, *5*, 5261–5268. [[CrossRef](#)]
36. Feng, X.; Chen, H.; Jiang, F. In-situ ethylenediamine-assisted synthesis of a magnetic iron-based metal-organic framework MIL-53(Fe) for visible light photocatalysis. *J. Colloid Interface Sci.* **2017**, *494*, 32–37. [[CrossRef](#)]

